Available online at www.sciencedirect.com
ScienceDirect
Journal of Sound and Vibration 315 (2008) 836–848
JOURNAL OF SOUND AND VIBRATION
www.elsevier.com/locate/jsvi

Noise reduction for compressors by modes control using topology optimization of eigenvalue

Jongchan Park, Semyung Wang*

Department of Mechatronics, Gwangju Institute of Science and Technology, 1 Oryong-dong, Buk-gu, Gwangju, 500-712, Republic of Korea

Received 29 April 2006; received in revised form 11 January 2008; accepted 19 January 2008
Handling Editor: L.G. Tham
Available online 18 April 2008

Abstract

Structural vibration is the most significant source of structure-borne noise. Avoiding severe resonances of the structures in order to reduce noise generation is the main interest of engineering fields.

This paper studied a typical example of the structure-borne noise reduction utilized in general engineering practices. Noise measurement and experimental modal analysis demonstrated that some resonance modes of the structure contribute highly to noise generation.

The reasons for the noise generation of the resonance modes were visualized through a finite element analysis. Mode control was employed to reduce the noise from the structure.

Topology optimization, in this research, was used to find the most effective structural configuration as present empirical designs fail to constrain various resonance modes. Design modifications based on the optimization result reduced the noise of the targeted mode without any significant design change in the structure. This example showed that the noise of the structure can be reduced by mode control using topology optimization.
© 2008 Elsevier Ltd. All rights reserved.

1. Introduction

Noise reduction has been a considerable research topic in recent years. Various approaches have been employed to deal with the noise or vibration problems as the source and transmission path or propagation is such a diverse phenomenon [1–7]. Among them, structure-borne noise [1,2] is generated by the vibrating structure and propagated through the ambient environment. Active noise control [3,4] is a common method utilized to reduce noise propagation but this method is too expensive to apply for mass production. Thus, passive noise control using dampers, absorption and insulation materials, which dissipate the vibrational energy or obstruct noise propagation, are preferred [5,7]. Another approach for avoiding the resonances of the structure is employed in this research to deal with the noise problem in existing engineering practices.

Compressors are the main source of the noise and vibration in air-conditioning units or refrigerators because the compressor undergoes a severe compression process. There are many noise sources of the

*Corresponding author. Tel.: +82 62 970 2390; fax: +82 62 970 2384.
E-mail address: smwang@gist.ac.kr (S. Wang).

0022-460X/$ - see front matter © 2008 Elsevier Ltd. All rights reserved.
doi:10.1016/j.jsv.2008.01.064

compressor such as gas pulsation, acoustic cavity, valves, and shell vibration [8,9]. However, regardless of the origin of the noise source, the fluctuating pressure of the air or noise generated and propagated from a structure for one dimension can be described as follows:

$$\nabla^2 p = \frac{\rho_0}{B}\frac{\partial^2 \rho}{\partial t^2} = \frac{1}{c^2}\frac{\partial^2 p}{\partial t^2} \tag{1}$$

where ρ_0 is density and B is the adiabatic bulk modulus of the medium. Eq. (1) is the linearized, homogeneous acoustic wave equation with the fluctuation pressure, $p(\bar{x}, t)$. Using velocity potential ϕ, and particle velocity u, the relation between the particle velocities and the fluctuation pressure is derived:

$$u = \nabla\phi = -\int \frac{1}{\rho_0}\vec{\nabla} p \, \mathrm{d}t \tag{2}$$

Actually, Eq. (2) shows that the fluctuation pressure is directly proportional to the particle velocities imparted by the vibrating structure [10] and that reduction of the vibration level of the structure will reduce the noise. With this basic concept, the research for reduction of the noise and vibration of a rotary compressor is conducted.

Accumulators are attached to the rotary compressor with a pipe, called a standpipe, and a strap as shown in Fig. 1. The standpipe is a passage for the refrigerant that is to be compressed. A strap fastens the accumulator to the compressor shell and reduces the vibration motion of the accumulator.

Some researchers have categorized the vibration of compressors in two ways: (1) as bending motions, and (2) as rigid body motions [8]. Usually, the latter have revealed little contribution to noise generation, which is the case for vibration motion of the accumulator under 3 kHz. However, using the directivity of the noise propagation from the compressor, recent research shows that accumulators are the main source of noise at some frequency ranges [9]. Noise radiated around the compressor is measured and confirms the previous research results in this research.

The optimization of the geometry as well as topology of the structural layout has a great impact on the performance of structures. Unlike other methods of optimization, a topology optimization technique can help

Fig. 1. Compressor assembly.

engineers who have to design a structure from scratch. This does not require a sophisticated initial design, but any geometry that describes the boundary conditions is enough to start in a topology optimization [11]. By considering the final pattern obtained from a topology optimization, engineers can obtain essential information for the initial design. For this reason, topology optimization is adopted extensively in diverse research and engineering fields such as structural [12–15], electromagnetic [16,17], and heat transfer [18].

In this research, topology optimization results provide a new design to constrain the target modes whereas the original design fails to the constrain resonant modes.

2. Experimental analysis

2.1. Sound measurement

To understand the noise generation and propagation of the compressor, sound pressure from the compressor was measured in an anechoic chamber as shown in Fig. 2. In Fig. 2, the most severe noise frequency range is from 600 Hz to 2 kHz, which became the target frequency range of this research.

Along with the averaged non-directional sound pressure, the directional contribution is checked. Sound pressures measured around the compressor at eight points are shown in Fig. 3. Sound pressure at 270 falling at the accumulator direction shows a much higher sound level at 1600 Hz center frequency on 1/3 octave band analysis. With regard to the structure-borne noise, it could be inferred that within this frequency range the structure has significant resonance modes, which contribute to the high-pressure level at 1.6 kHz. Modal tests are then conducted in order to find the structural resonance of the compressor.

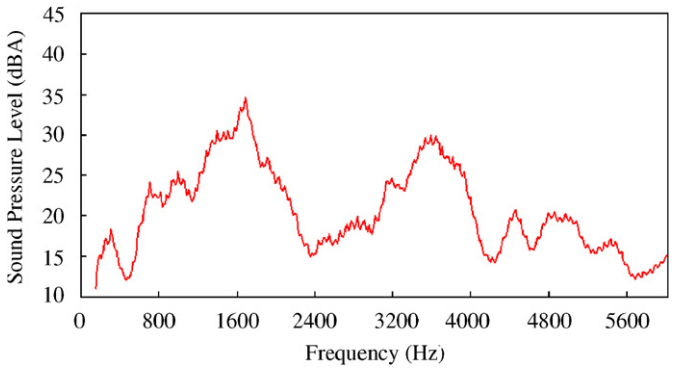

Fig. 2. Sound pressure level of the compressor.

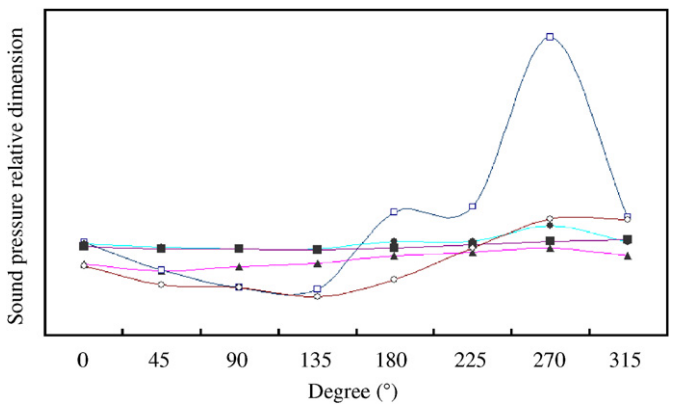

Fig. 3. 1/3 octave analysis of the sound pressure around the compressor: ○ 800 Hz, ▲ 1 kHz, ● 1.25 kHz, □ 1.6 kHz, ■ 2 kHz.

2.2. Modal test

Two kinds of modal tests are conducted to investigate the role of the present strap in compressor assembly: (1) without the strap and (2) with the strap installed. Both the modal tests demonstrate that under a frequency of 2 kHz the main resonance modes are the rigid body motions of the accumulator, which are caused by the deformation of the standpipe and first shell bending of the accumulator, which occurs at 3.3 kHz. However, this is far beyond the targeted frequency range, 600 Hz–2 kHz. This result implies that the rigid body motions of the accumulator under 2 kHz contribute highly to the directivity of sound pressure level at 1.6 kHz on the 1/3 octave band analysis shown in Fig. 3.

Experimental modal analysis results are given and compared with the Finite element (FE) analysis results in Table 1. Among them, two mode shapes at 908 and 1744 Hz are given in Fig. 4 for the strap-uninstalled case.

In Fig. 4, the pivot point of the two modes is the strap, which is intended to reduce the vibration motion of the accumulator. Therefore, this provides evidence that the present strap and stand pipe are inadequate to constrain or reduce those vibration motions. Furthermore, those resonant frequencies correspond to the highest sound level frequencies as shown in Fig. 2.

Table 1
Modal analysis results for strap un-installed assembly

Mode	Test (Hz)	Analysis (Hz)	Error (%)
1st	42	43	2
2nd	52	53	2
3rd	379	361	5
4th	390	397	2
5th	426	406	7
6th	472	471	1
7th	528	484	8
8th	*908*	*933*	*2*
9th	1548	1553	1
10th	*1744*	*1702*	*2*

The italic values in 8th and 10th modes represent strap-uninstalled case.

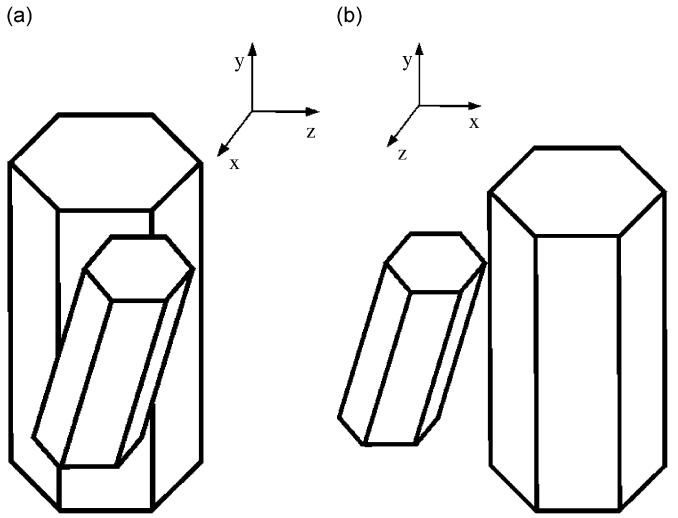

Fig. 4. Mode shapes of the rigid body motion of the accumulator in modal test: (a) 908 Hz, (b) 1744 Hz.

3. Finite element analysis

A finite element model of the compressor assembly, which is composed of all the inner parts such as the shaft, stator, rotor, and bearings is built for the FE analysis and design change using CAE. Figs. 5 and 6 illustrate the vibration mode of the strap-uninstalled case and strap-installed case, respectively. The spectrum

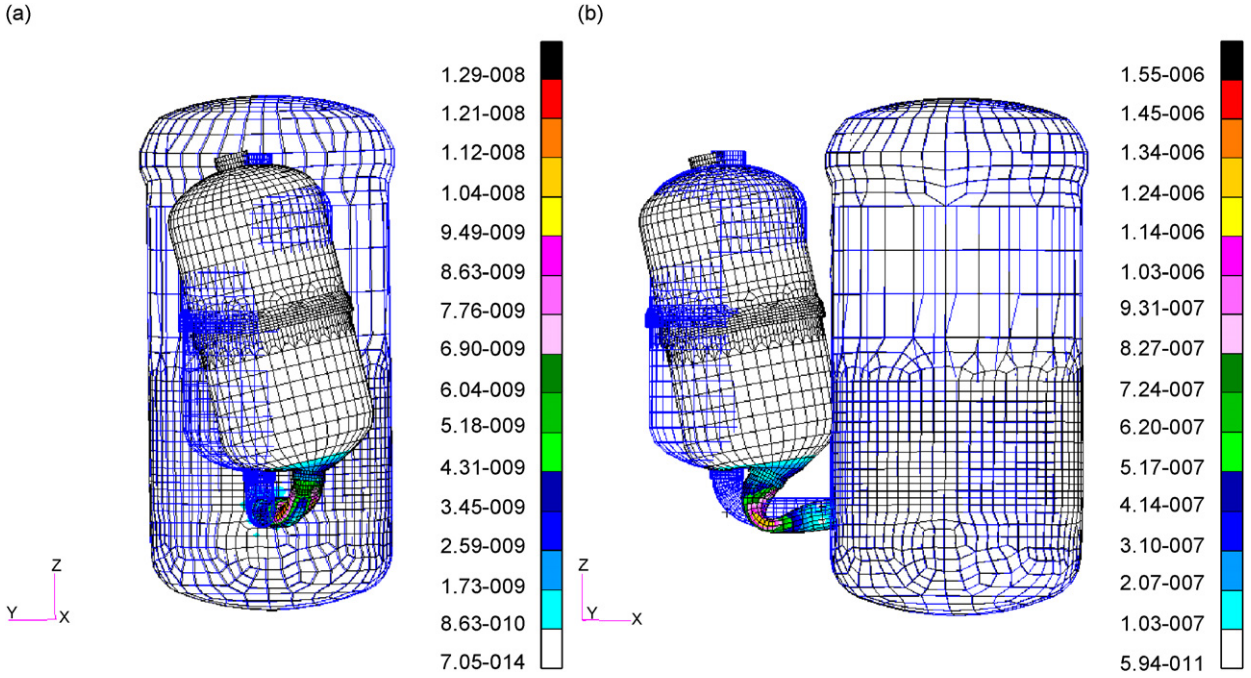

Fig. 5. Mode shapes of the rigid body motion of the accumulator in FE analysis without a strap: (a) 933 Hz and (b) 1702 Hz.

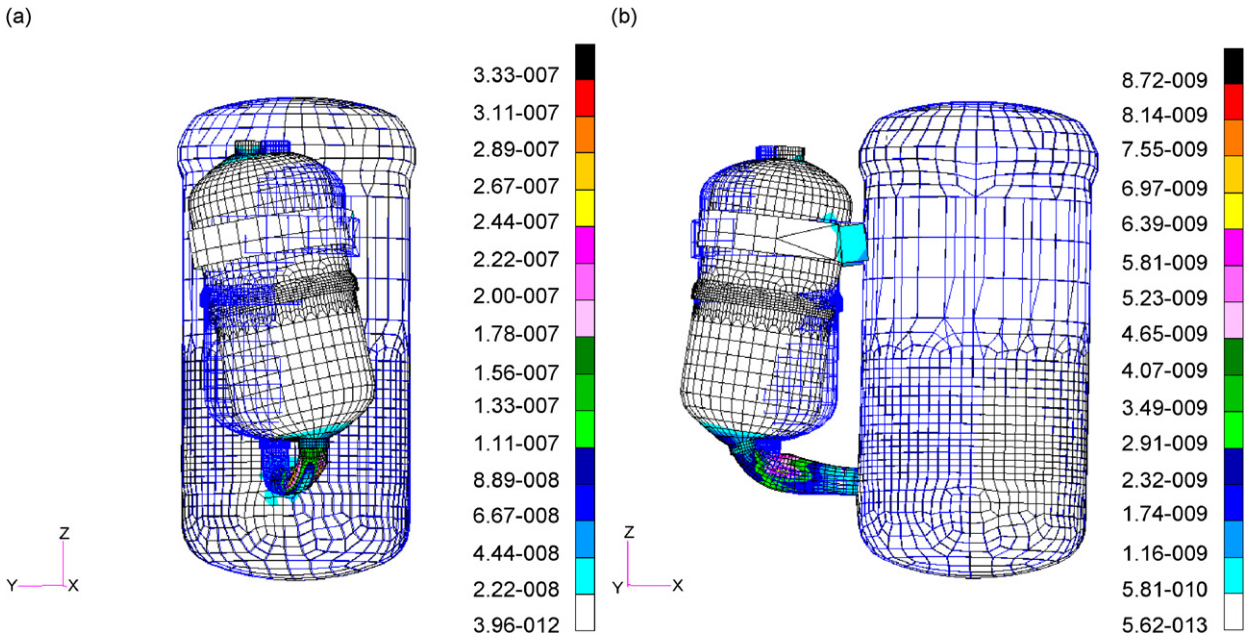

Fig. 6. Mode shapes of the rigid body motion of the accumulator in FE analysis with strap: (a) 963 Hz and (b) 1742 Hz.

Table 2
Modal analysis results for strap installed assembly

Mode	Test (Hz)	Analysis (Hz)	Error (%)
1st	231	234	1
2nd	390	375	4
3rd	504	448	11
4th	526	483	8
5th	*945*	*963*	*2*
6th	1428	1382	3
7th	1558	1673	7
8th	*1746*	*1742*	*1*

The italic values in 5th and 8th modes represent strap-installed case.

shows distribution of the strain at those modes. In Figs. 5 and 6, most of the deformation denoted by the spectrum level, not the translation, take places at the stand pipe. It implies that those resonance modes are due to the bending deformation of the stand pipe.

Tables 1 and 2 show the comparison of resonance modes between the modal test and FE analysis results for strap uninstalled and strap installed, respectively. The 8th and the 10th modes for the strap-uninstalled case in Table 1 fall at the 5th and the 8th modes for the strap-installed case in Table 2. This comparison demonstrates that the present strap fails to constrain the most dominant modes of noise generation. Considering the mode shapes in Figs. 4 and 5, as well as the frequency change after installation of the strap, it can be inferred that the present strap does not work for those modes.

As shown in Figs. 5 and 6, most of the strain takes place at the stand pipe and the other parts of the structure undergo just rigid body translation. In order to avoid those modes strengthening the standpipe by increasing the thickness or changing the material did not show any improvement, though there was a minor frequency shift. Thus, a design change for the attachment of the accumulator to the compressor using topology optimization was conducted.

4. Topology optimization for the eigenvalue problem

4.1. Design sensitivity formulation for the eigenvalue problem

In the density method, a topology optimization method, the density function η_i in each finite element is considered as design variables. The relationship between the effective material properties and the given isotropic material properties is [11,12]

$$\mathbf{E} = \eta^p E_0 \tag{3}$$

where $\mathbf{E}_0$ is the initial material matrix defined as E and v, Young's modulus and Poisson's ratio of the given isotropic material, respectively.

For the eigenvalue problem, the structural equation is

$$a_\Omega(\mathbf{y}, \bar{\mathbf{y}}) = \zeta d_\Omega(\mathbf{y}, \bar{\mathbf{y}}) \quad \text{for all } \bar{\mathbf{y}} \in Z \tag{4}$$

where ζ is the eigenvalue, $\mathbf{y}$ is the eigenvector with respect to ζ and Z is the space of kinematically admissible displacement.

In the case of a simple eigenvalue problem, the eigenvalue ζ is differentiable and the corresponding Eigenvector $\mathbf{y}$ is also differentiable.

The strain energy bilinear form and the kinetic energy bilinear form are written as

$$\begin{aligned} a_\Omega(\mathbf{y}, \bar{\mathbf{y}}) &= \int_\Omega \boldsymbol{\varepsilon}_i^{\mathrm{T}} \mathbf{E} \bar{\boldsymbol{\varepsilon}}_i \, \mathrm{d}\Omega \\ d_\Omega(\mathbf{y}, \bar{\mathbf{y}}) &= \int_\Omega \rho \mathbf{y}^{\mathrm{T}} \bar{\mathbf{y}} \, \mathrm{d}\Omega \end{aligned} \tag{5}$$

where ρ is the effective density and $\boldsymbol{\varepsilon}$ is strain. The relationship between ρ and ρ_0, the given density, is denoted as

$$\rho = \eta\rho_0 \tag{6}$$

The derivatives of $\mathbf{E}$ and ρ with respect to the design variable η are

$$\begin{aligned}\frac{\partial \mathbf{E}}{\partial \eta} &= p\eta^{p-1}\mathbf{E}_0 = \frac{\rho}{\eta}\eta^p\mathbf{E}_0 = \frac{\rho}{\eta}\mathbf{E}\\ \frac{\partial \rho}{\partial \eta} &= \rho_0 = \frac{1}{\eta}\eta\rho_0 = \frac{1}{\eta}\rho\end{aligned} \tag{7}$$

The derivatives of the strain energy bilinear form and the kinetic energy bilinear form with respect to design variable are written as

$$\begin{aligned}[a_\Omega(\mathbf{y},\bar{\mathbf{y}})]' &= \int_\Omega \boldsymbol{\varepsilon}_i^{\mathrm{T}}\frac{\partial \mathbf{E}}{\partial \eta}\bar{\boldsymbol{\varepsilon}}_i\,\mathrm{d}\Omega = \frac{p}{\eta}\int_\Omega \boldsymbol{\varepsilon}_i^{\mathrm{T}}\mathbf{E}\bar{\boldsymbol{\varepsilon}}_i\,\mathrm{d}\Omega = \frac{p}{\eta}a_\Omega(\mathbf{y},\bar{\mathbf{y}})\\ [d_\Omega(\mathbf{y},\bar{\mathbf{y}})]' &= \int_\Omega \frac{\partial \rho}{\partial \eta}\mathbf{y}^{\mathrm{T}}\bar{\mathbf{y}}\,\mathrm{d}\Omega = \frac{1}{\eta}\int_\Omega \rho\mathbf{y}^{\mathrm{T}}\bar{\mathbf{y}}\,\mathrm{d}\Omega = \frac{1}{\eta}d_\Omega(\mathbf{y},\bar{\mathbf{y}})\end{aligned} \tag{8}$$

The first variation of Eq. (4) is

$$[a_\Omega(\mathbf{y},\bar{\mathbf{y}})]' = \zeta' d_\Omega(\mathbf{y},\bar{\mathbf{y}}) + \zeta[d_\Omega(\mathbf{y},\bar{\mathbf{y}})]' \tag{9}$$

Since Eq. (4) holds for all $\bar{\mathbf{y}} \in Z$, this equation may be evaluated with $\mathbf{y} = \bar{\mathbf{y}}$. Using the normalizing condition, $d_\Omega(\mathbf{y},\mathbf{y}) = 1$, Eq. (9) is rewritten as

$$\zeta' = [a_\Omega(\mathbf{y},\mathbf{y})]' = \zeta[d_\Omega(\mathbf{y},\mathbf{y})]' = \frac{\rho}{\eta}a_\Omega(\mathbf{y},\mathbf{y}) - \frac{1}{\eta}\zeta d_\Omega(\mathbf{y},\mathbf{y}) \tag{10}$$

4.2. Optimization problem and result

FE models are constructed for the modal analysis and topology optimization. For the former case, analysis results are deeply affected by the mesh size. Conversely, for the topology optimization, the optimization procedure needs both analysis and sensitivity calculations. Therefore, the analysis model is reduced to a design model because the size of the analysis model is too large to be used for the optimization. Fig. 7 shows the analysis model and design model, respectively. In the design model, the compressor shell part is regarded as a rigid wall. Normal mode analysis of the design model gave evidence that a reduction of the model and an assumption of the rigid wall of the compressor shell did not significantly affect the target modes.

The design variable domain, as shown in Fig. 8, is set between the accumulator and the rigid wall in order to find the most efficient structural configuration that maximizes the target resonance modes.

The topology optimization is written as

$$\begin{aligned}&\text{Maximize} && \text{Eigenvalue of the resonance mode}\\ &\text{Subject to} && V \leqslant 0.1\,V_0\end{aligned} \tag{11}$$

where V is the volume of the design variable at each iteration and V_0 is the initial volume. A commercial design optimization tool (DOT from Vanderplaats R&D) checks convergence of the problem using the sequential linear programming (SLP).

Using only 10% of the design domain volume, the optimization problem is solved. Fig. 9 shows the history of the objective function of the optimization procedures. Fig. 9 shows that resonance frequency is shifted beyond 2.5 kHz. Objective function, resonance frequency, has the value around 1.1 kHz at the starting iteration because the densities of the design variables are, initially, set to 10% of the given density.

Fig. 10 shows the evolution history of the optimization procedures. Four iterations among the total 51, shown in Fig. 10, illustrate the sensitivity change of the design variables for the restriction of the target modes. Density transition of design variables shown in Fig. 10(d) implies the lower part and upper part are the most important.

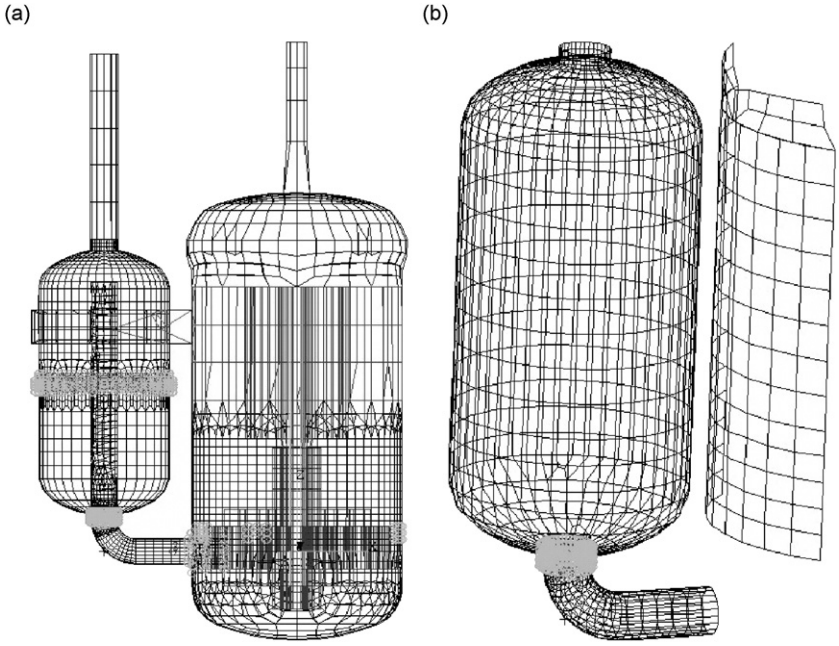

Fig. 7. Analysis and design models: (a) analysis model and (b) design model for optimization.

The selected elements from final optimization results in Fig. 11 show two separate parts at the upper and lower region of the accumulator. Elements at the upper parts correspond to the current strap. However, elements at the lower part of the accumulator indicate that there has to be a new structure to restrict the resonance mode of the accumulator.

4.3. Reanalysis of the optimization results and considerations

Fig. 12 illustrates the analysis results of the new model embodying the optimization results. For the optimization model target frequencies are shifted above 2.5 kHz. However, for the new model the resonance mode of the accumulator occurs at 2141 Hz which is lower than the optimization results. The difference of the analysis results between the optimization model and reconstructed model comes from the re-mesh of the model and removing low-density element from the design variable domain in Figs. 10(d). Also, the upper part of the optimization results is not applied to the reanalysis model because there already exist a current strap and the optimized shape of the upper part is just increasing the stiffness of the present strap.

Finite element analysis employing optimization results of only the upper part showed that an increase in stiffness of the upper strap was not sufficient for the constraint of the target modes. And, strengthening the standpipe was not sufficient also. Significant improvement on the performance shown in Fig. 12 was achieved only with the additional installation of the lower part as shown in the optimization results.

Aside from the local bending deformation of the standpipe that predominates the mode shape of the resonance mode, there exists some deformation of the accumulator shell in Fig. 12. It shows the difference of the mode of Fig. 6(b) and Fig. 12. Deformation of the accumulator shell shown in Fig. 12 implies that those modes occur at a comparatively high-frequency range.

5. Verification with experiment

Structural optimization results show that there should be two separate substructures between the accumulator and compressor shell. The first exists already at the same place with the current strap and the latter is suggested to be constructed to the lower part of the accumulator. FE analysis results of the new model constructed following the optimization results verified optimization results.

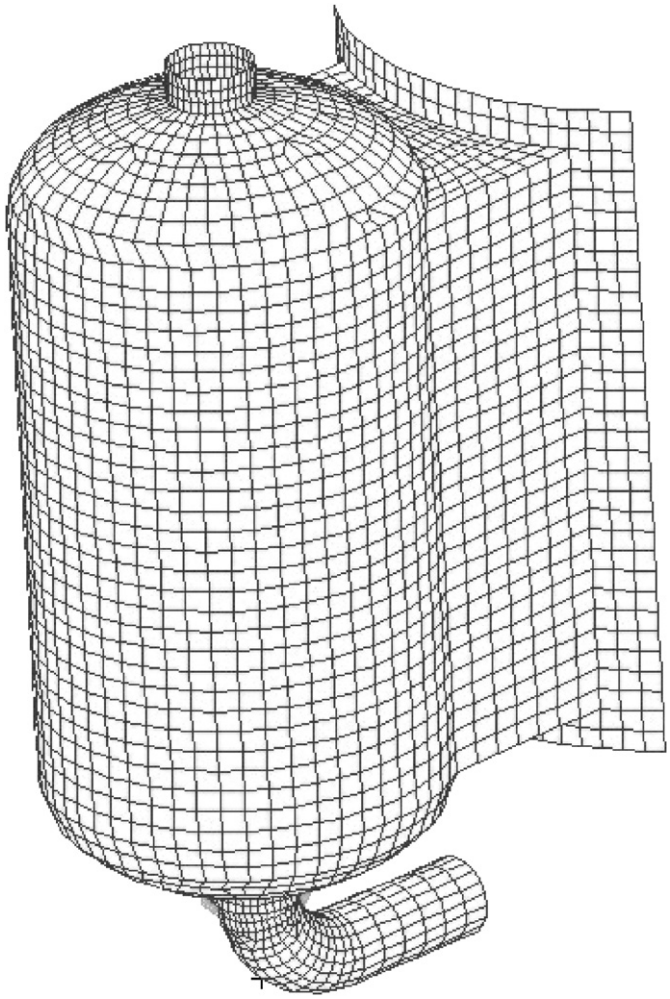

Fig. 8. Design variable domain.

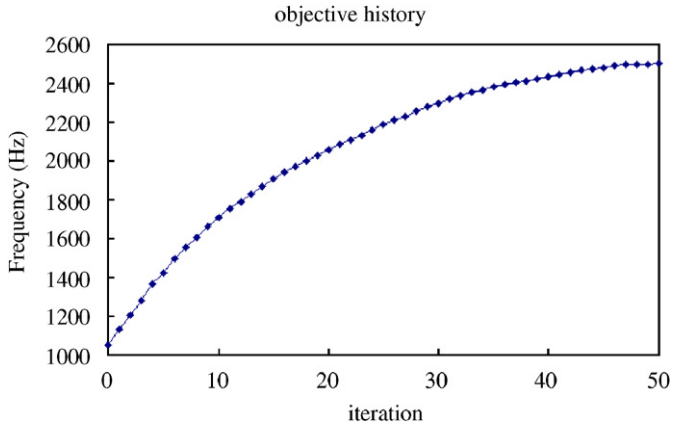

Fig. 9. History of objective function.

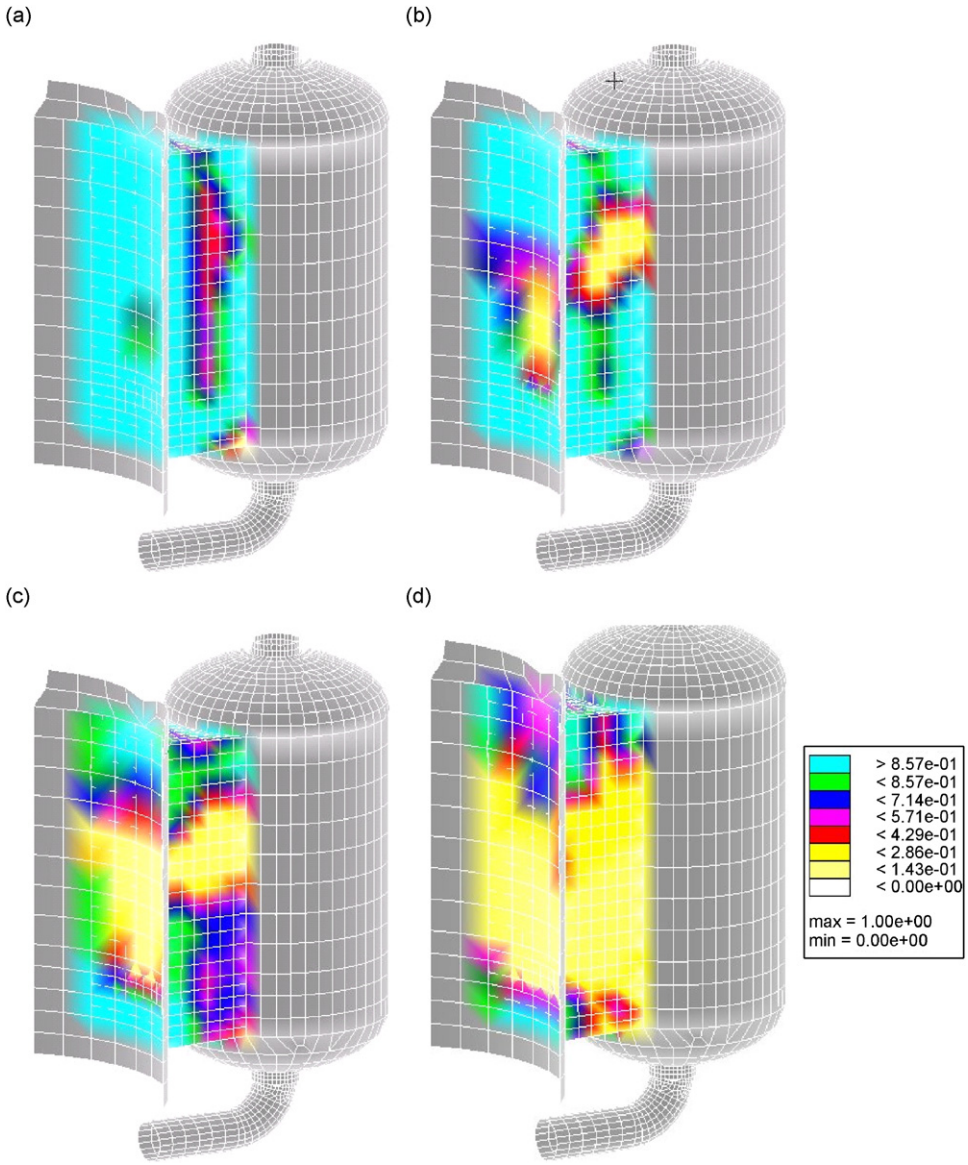

Fig. 10. Evolution history of design variables in the optimization procedures: (a) 9th iteration, (b) 26th iteration, (c) 41st iteration and (d) the final results and density spectrum.

To investigate the effect of the inserted block at the lower part of the assembly, modal tests and sound measurement experiments were carried out. The obtained shape of the optimization results shown in Fig. 13(a) makes it difficult to install the block into the compressor assembly. Thus, taking the assembling process into consideration, the modified block shown in Fig. 13(b) is fabricated. The original optimization results of the lower part, modified block, and modified block-installed assembly are provided in Figs. 13(a), (b) and (c), respectively.

In Fig. 14, the FRF of the impact tests are compared. As stated previously, the present strap does not work for the resonance mode at 1.7 kHz as compared to the no-strap case.

Significant frequency shift and reduction of the vibration level is accomplished only with the installation of the block shown in Fig. 13(c). Generally, the resonance shift from the frequency range of high noise by stiffening the structure is very effective methodology [19,20]. However, as noted in the modal experiment in Fig. 14, design modifications not only shift resonance frequency but also reduce the vibration level.

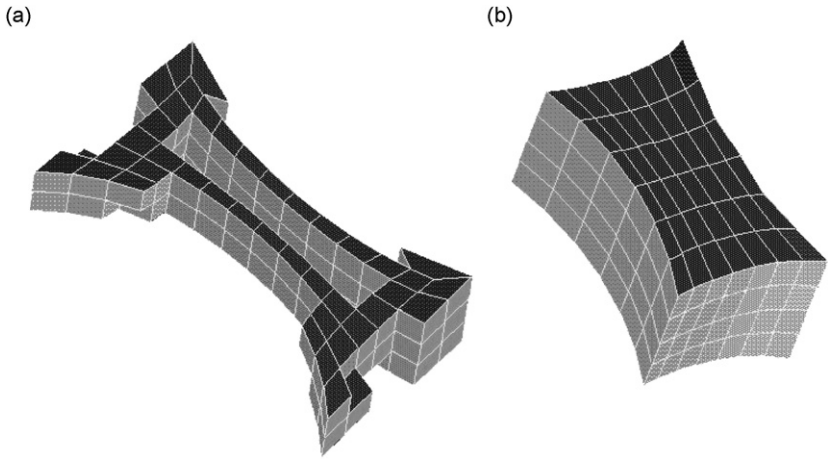

Fig. 11. Selected elements from the topology optimization: (a) upper part and (b) lower part.

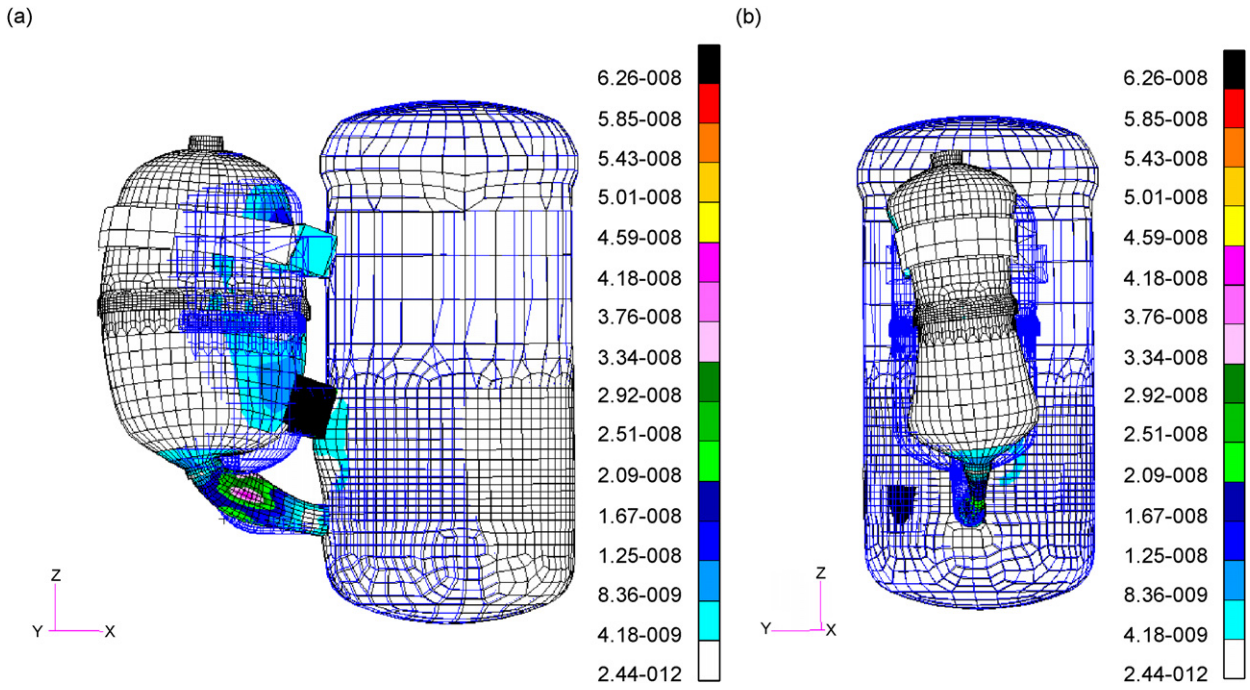

Fig. 12. Distribution of the strain and vibration shape of new model at 2141 Hz: (a) side view and (b) front view.

Increased damping or reduced vibration level shown in Fig. 14 is considered to result from assembling the blocks with a bolt which has some interfacial contact surfaces. It is well known that joints and fasteners have a significant effect on the dynamic behavior of assembled mechanical structures [21,22]. More details of the increased damping go beyond the scope of this research.

In Fig. 15, sound reduction according to the installation of the block at 1.6 kHz on the 1/3 octave band is presented. As noted in Fig. 15, effective noise reduction is achieved around the targeted frequency range at which dominant structural resonances disappear as demonstrated in the modal test results in Fig. 14.

In conclusion, noise reduction illustrated in Fig. 15 along with the experimental modal analysis demonstrates the effectiveness of employing the topology optimization to design a functional structure. The following comment is addressed for a stress.

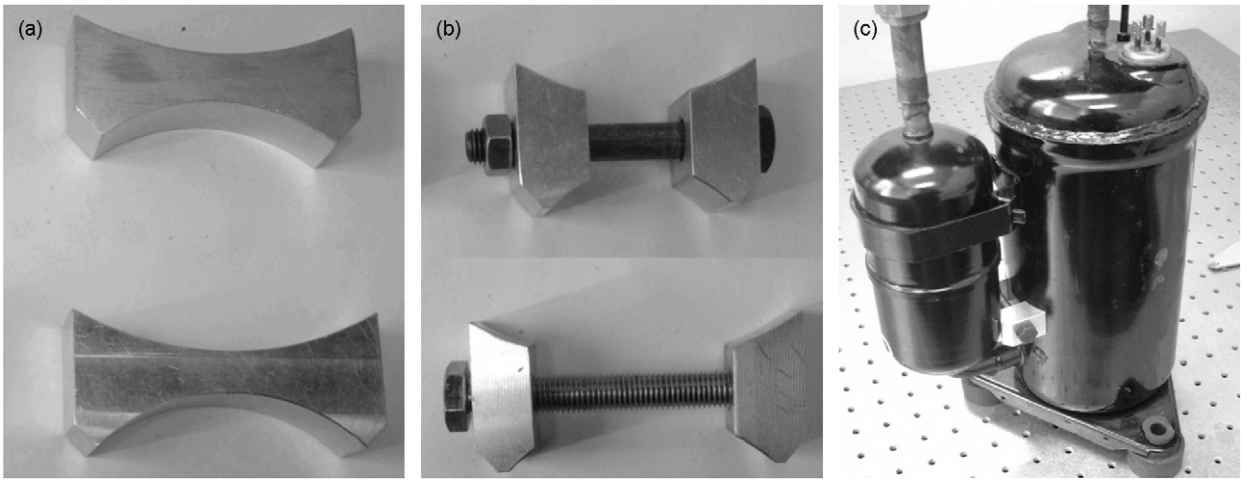

Fig. 13. Practical application of the optimization results: (a) results of the lower part optimization, (b) modified block (lower part) and (c) block applied model.

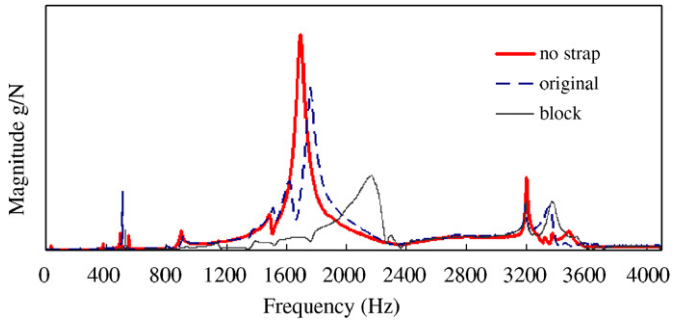

Fig. 14. FRF comparisons between without strap model (no strap) and strap installed model (original) and block-installed model (block).

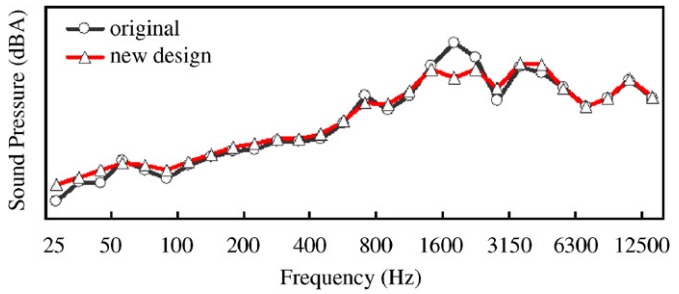

Fig. 15. Sound pressure comparisons according to the block installation.

(1) Topology optimization can be a useful methodology to design a structure from the scratch when the current system has a missing part or a wrong design.
(2) Engineers or researchers using this methodology should be careful to find the basic meaning or purpose of the optimization results not to stick to the seeming shape. For example, the concave block-shaped structure in the optimization results is modified into bolted two separate blocks in order to the restrict the target resonance mode.

6. Conclusions

Structure-borne noise reduction has been studied for engineering practice through modal analysis and structural optimization. Sound measurement test was carried out to find the target frequency range, which contributes highly to noise propagation. Also, directivity from the sound spectrum indicates that the accumulator is a significant component in the objective frequency range.

Experimental modal analysis is used to figure out the dynamic characteristics of the rotary compressor. Two of the obtained resonance modes correspond to the highest peaks in the sound spectrum, which implies that the constraint of those modes will reduce the noise level.

A finite element model with all components of the compressor assembly is constructed and used for modal analysis. Analyses of these results visualize the reason for the target resonance modes. Topology optimization of eigenvalue is used to avoid those resonance modes without significantly changing the present structure. Using the topology optimization results, a block-shaped component is inserted between the accumulator and the compressor. Sound measurement tests and modal tests with the block-inserted model verify the topology optimization results. The resulting sound spectrum verifies that a reduced noise level is obtained in the target frequency range.

References

[1] K.W. Ngai, C.F. Ng, Structure-borne noise and vibration of concrete box structure and rail viaduct, *Journal of Sound and Vibration* 255 (2002) 281–297.
[2] S.H. Ko, W.S. Seong, S.W. Pyo, Structure-borne noise reduction for an infinite, elastic cylindrical shell, *Journal of the Acoustical Society of America* 109 (2001) 1483–1495.
[3] S. Snyder, C.H. Hansen, Active noise control in ducts: some physical insights, *Journal of the Acoustical Society of America* 86 (1989) 184–194.
[4] B. Wang, C.R. Fuller, E.K. Dimitriadis, Active control of noise transmission through rectangular plates using multiple piezoelectric or point force actuators, *Journal of the Acoustical Society of America* 90 (1991) 2820–2830.
[5] C. Wassilieff, Improving the noise reduction of picket barriers, *Journal of the Acoustical Society of America* 84 (1988) 645–650.
[6] D.B. Callaway, R.D. Lemmerman, A comparison between model study tests and field measurements on an aircraft test-cell silencer, *Journal of the Acoustical Society of America* 25 (1953) 429–432.
[7] G.G. Tseo, Estimating the noise reduction of wall structures of enclosures, *Journal of the Acoustical Society of America* 52 (1972) 1573–1578.
[8] C.N. Johnson, Noise study of practical horsepower, rotary vane, refrigerant compressors, *Proceedings of the 1972 International Compressor Engineering Conference at Purdue*, 1972, pp. 74–82.
[9] J.D. Kim, B.H. Kwon, Noise reduction of a rotary compressor using structural modification of the accumulator, *Proceedings of the 1998 International Compressor Engineering Conference at Purdue*, 1988, pp. 355–360.
[10] L.L. Beranek, I.L. Ver, *Noise and Vibration Control Engineering*, Wiley, New York, 1992.
[11] M.P. Bendsoe, *Optimization of Structural Topology, Shape, and Material*, Springer, Berlin, Heidelberg, 1995.
[12] J. Lee, S. Wang, A. Dikec, Topology optimization for the radiation and scattering of sound from thin-body using genetic algorithms, *Journal of Sound and Vibration* 276 (2004) 899–918.
[13] S. Cho, C.Y. Par, Y.H. Park, S.Y. Hong, Topology design optimization of structures at high frequencies using power flow analysis, *Journal of Sound and Vibration* 298 (2006) 206–220.
[14] J.S. Jensen, Topology optimization problems for reflection and dissipation of elastic waves, *Journal of Sound and Vibration* 301 (2007) 319–340.
[15] G.Y. Cui, K. Tai, B.P. Wang, Topology optimization for maximum natural frequency using simulated annealing and morphological representation, *AIAA Journal* 40 (2002) 586–589.
[16] S. Wang, J. Kang, Topology optimization of nonlinear magnetostatics, *IEEE Transactions of Magnetics* 38 (2) (2002).
[17] S. Wang, J. Kang, J. Noh, Topology optimization of a single-phase induction motor for rotary compressor, *IEEE Transactions on Magnetics* 40 (3) (2004).
[18] O. Sigmund, Topology optimization in multiphysics problems, *Proceedings of the Seventh AIAA/USAF/NASA/ISSMO Symposium on MAO* (1998) 1492–1500.
[19] M. Ruzzene, A. Baz, Finite element modeling of vibration and sound radiation from fluid-loaded damped shells, *Thin-Walled Structures* 36 (2000) 21–46.
[20] R.S. Ming, J. Pan, M.P. Norton, M. Teh, The passive control of tonal sound radiation from vibrating structures, *Applied Acoustics* 60 (2007) 313–326.
[21] M.H. Mayer, L. Gaul, Segment-to-segment contact elements for modeling joint interfaces in finite element analysis, *Mechanical Systems and Signal Processing* 21 (2007) 724–736.
[22] H. Ahmadian, H. Jalali, Generic element formulation for modeling bolted lap joints, *Mechanical Systems and Signal Processing* 21 (2007) 2318–2334.